Northumbria Research Link

Northumbria
University
NEWCASTLE

Ultrahigh Frequency Surface Acoustic Wave Sensor with Giant Mass-loading Effect on Electrodes

Zhe Chen,[‡a] Jian Zhou,[‡*a] Hao Tang,[b] Yi Liu,[c] Yiping Shen,[c] Xiaobo Yin[a], Hongshuai Zhang,[b] Jianhui Wu,[a] Xianglong Shi,[d] Yiqin Chen,[a] Yongqing Fu,[e] Huigao Duan.[*a]

a. State Key Laboratory of Advanced Design and Manufacturing for Vehicle Body, College of Mechanical and Vehicle Engineering, Hunan University, Changsha 410082, P.R. China.

b. State Key Laboratory of Chemo/Bio-Sensing and Chemometrics, College of Chemistry and Chemical Engineering, Hunan University, Changsha 410082, P.R. China.

c. Hunan Provincial Key Laboratory of Health Maintenance for Mechanical Equipment, Hunan University of Science and Technology, Xiangtan 411201, P.R. China.

d. Address here Beijing Aerospace Micro-electronics Technology Co., Beijing 100854, P.R. China.

e. Faculty of Engineering and Environment, Northumbria University, Newcastle upon Tyne, NE1 8ST, United Kingdom.

KEYWORDS : ultrahigh frequency; surface acoustic wave; IDT; mass-loading effect; sensors

ABSTRACT: Surface acoustic wave (SAW) devices are widely used for physical, chemical and biological sensing applications, and their sensing mechanisms are generally based on frequency changes due to mass loading effect at the acoustic wave propagation area between two interdigitated transducers (IDTs). In this paper, a new sensing mechanism has been proposed based on significantly enhanced mass-loading effect generated directly on Au IDT electrodes, which enables significantly enhanced sensitivity compared with that of the conventional SAW devices. The fabricated ultrahigh frequency SAW devices show significant mass-loading effect on the electrodes. With Au electrode thickness increased from 12 nm to 25 nm, Rayleigh mode resonant frequency decreases from 7.77 GHz to 5.93 GHz, while that of the higher longitudinal leaky SAW decreases from 11.87 GHz to 9.83 GHz. The corresponding mass sensitivity of 7309 MHz·mm2·μg^{-1} (Rayleigh mode) is ~8.9×10^{11} times larger than that of a conventional quartz crystal balance (with a frequency of 5 MHz) and ~1000 times higher than that of conventional SAW devices (with a frequency of 978 MHz). Trinitrotoluene concentration as low as 4.4×10^{-9} M (mol·L^{-1}) can be detected using the fabricated SAW sensor, proving its giant mass-loading effect and ultrahigh sensitivity.

Sensors based on surface acoustic waves (SAWs) have been considered as powerful tools to measure physical parameters, such as temperature, force, acceleration, humidity, electric and magnetic fields and potentials, [1-5] or chemical and biochemical values, such as concentrations of gas, vapor, ion, DNA and protein.[6-9] Bulk piezoelectric materials such as quartz, $LiNbO_3$ and $LiTaO_3$ have usually been the substrates of choice for SAW sensing applications, mainly due to their large piezoelectric coefficients and electromechanical coupling coefficients, thus high energy transduction coefficients.[10, 11] In addition, smooth surfaces and good piezoelectric properties of these bulk substrates are beneficial to micro-fabrication of the SAW IDTs which lead to high quality factors (Q) and good sensing accuracy of SAW devices.[12]

Generally for the delay-line based SAW devices, the sensing area of the SAW sensor is the acoustic wave propagation region between two IDTs.[13] When there are mass loading effects or changes in electrical, physical and chemical properties of the sensing areas, the resonant frequencies and phase angles of SAW sensors will be changed.[14] The mass sensitivity of SAW sensors is generally based on the following formula,[15]

$$\Delta f = \frac{C f_0^{\,2}}{A}\Delta m \quad (1)$$

where f_0 is the resonant frequency of SAW device, Δf is the frequency shift, C is a constant, A is the active surface area and Δm is the mass loading (or change). In order to increase the sensitivity of SAW devices, we need to either increase the resonant frequency f_0 or decrease the wavelength based on the relationship of $f_0 = c/\lambda$, where, c is the acoustic wave velocity and λ is the SAW wavelength. However, it is becoming difficult when the SAW frequency is increased up to GHz level, as the distance between the two ports of SAW IDTs will need to be several micrometers or even sub-micrometer scale, and the wavelength of the IDT will be decreased to nano-scale.[16] Otherwise, if the distance between the two ports of SAW IDTs is quite large for the SAW device with a wavelength in sub-micron scale, there will be significant propagation loss of SAWs and weakened signal quality.

In this paper, we investigate a new sensing mechanism, which is based on the significant mass-loading effect, directly on the IDT electrodes of SAW resonators. Theoretical, simulation and experimental results show that frequency shifts due to the mass-loading effects directly on

top of IDT electrodes are significantly larger than those on the acoustic wave propagation area, mainly due to the significant changes of acoustic fields at the exciting regions of the SAWs. This phenomenon becomes more significant when the frequency is above GHz. In this study, using an optimized nanofabrication process, ultrahigh frequency SAW devices with frequencies up to 12 GHz are fabricated, and their high mass sensing sensitivity is demonstrated for trinitrotoluene (TNT) detection.

Theoretical calculation and experimental

FEM simulation and theoretical calculation

Firstly, we performed simulations of mass-loading effects on IDT electrodes using a finite element analysis (FEA) method with a commercial COMSOL 5.3a software. To investigate the differences of frequency shifts between the mass loading at acoustic wave propagation area (Figure 1 (a)) and that directly on IDT electrodes (Figure.1(b)), a complete two-dimensional (2D) model was established and a time-domain analysis was performed (Figure.1 (c)). Piezoelectric layer was chosen as $LiNbO_3$ and its thickness was set as 2λ with a fixed bottom boundary condition. The two sides of the $LiNbO_3$ was assigned to be in low reflection boundary conditions. A free and zero charge boundary condition was assigned to the top surface of the piezoelectric $LiNbO_3$ layer. The electrode material was Au with a thickness of 12 nm, and the boundary between the $LiNbO_3$ and Au was assigned to be free and continuous. The wavelength λ was set as 400 nm. The SAW IDTs were consisted of 80 pairs of fingers with an aperture (W) of 20λ and each IDT has 50 reflectors. The distance between the two IDTs was 40λ. To simulate frequency shifts due to the mass loading within the acoustic wave propagation area, Au film was set as the mass loading material with an area of 40λ × 20λ and thicknesses of 6 nm and 13 nm, corresponding to mass loadings at acoustic wave propagation area of 1.15 μg·mm^{-2} and 2.51 μg·mm^{-2}, respectively. On the other hand, to simulate frequency shifts due to the SAW mass loading directly on the IDT electrodes, the Au film was added on the SAW IDTs with thicknesses of 6 nm and 13 nm. Because the SAW device has 80 pairs of IDT fingers, the mass loadings were estimated to be ~1.15 μg·mm^{-2} and 2.51 μg·mm^{-2}, respectively.

A periodic 2D piezo plane strain modeling was further conducted (Figure.1(d)) to investigate the mechanism of electrode mass-loading effect on SAW propagation properties, such as resonant frequency, wave modes, particle vibration, surface perturbation and geometrical variations of the electrode shape of the SAW devices. SAW IDTs are periodic in nature, alternatively consisting of positive and negative potentials. Thus, one period of the electrode would be sufficient to illustrate the resonance characteristics of the SAW resonator. For this type of simulation, the thicknesses of Au electrode were chosen as 10, 20, 30, 50, 80, 100, 120, 150, 200 nm to demonstrate different mass loading effects on the IDT electrodes. The wavelengths were set as 10 μm and 200 nm to study the differences of mass loading effects between the micro-scale IDTs and nano-scale IDTs. The substrates were set as $LiNbO_3$ or AlN/Diamond in order to investigate the substrate influences.

To verify the correctness and accuracy of simulation results and theoretically analyze the relationship between mass loading directly on IDT fingers and the performance of super-high frequency $LiNbO_3$ SAW device, finite element model/boundary element model (FEM/BEM) method was used. The 2D numerical model for the simulation of a periodic array of Au electrodes on a semi-infinite half space was used. The Au was set as a thin layer. The $LiNbO_3$ was set as an isotropic half space during simulation because its thickness is much larger than the SAW wavelength. Green's function for a semi-infinite piezoelectric substrate was employed, where only charges at the electrode/substrate interfaces (z=0) were considered.[17] The Green's function is described using the following equation:

$$\begin{pmatrix} u(x) \\ \varphi(x) \end{pmatrix} = \sum_{j=1}^{N_e} \int_{c_j-a_j}^{c_j+a_j} G_\gamma^p(x-x') \begin{pmatrix} t_s(x') \\ \sigma(x') \end{pmatrix} dx' \qquad (2)$$

where u is particle displacements, φ is the electric potential, t the mechanical stress components in z-direction, σ the charges at the interface, N_e is the number of electrodes for one period of the array, c_j is the x coordinate of the electrode center, and a_j is the half electrode width for the j^{th} electrode of the elementary period. $G_\gamma^p(x)$ is the periodic harmonic Greens function (which was first introduced by Plessky et al).[18]

The next simulation step was to integrate the electrode's mechanical behavior into the above system. Using a similar approach as described in Ref[18], we assumed that the metallic electrodes are homogeneous, isotropic, and elastic (ρ is the mass density; λ and μ are the Lame constants).[19] Each electrode was discretized into triangular finite elements (linear or quadratic interpolation can be used) and the FEA was used to derive linear equations which are related to the nodal displacements and force vectors (**U**, **F**):

$$(\mathbf{K} - \omega^2\mathbf{M})\mathbf{U} = \mathbf{F} \qquad (3)$$

where **K**, **M** are stiffness and mass matrix, respectively, and **F** is computed from stresses $\mathbf{t}_s$ according to:

$$F_i = \int_{\Gamma_{es}} \boldsymbol{t_s}(x) W_i(x) dx \qquad (4)$$

where $W_i(x)$ is the FEA basis function associated with node i. The derivation process of the formula and calculation method was referred to our previous work.[19]

Finally, the current flowing into the j-finger can be calculated using the following equation:

$$I_j = \int_{-a_j}^{a_j} \frac{\partial \sigma(x)}{\partial x} dx \qquad (5)$$

Once the current flowing into every single finger was obtained, we then calculated the admittance matrix of the SAWs with arbitrary numbers of electric ports according to the circuit theory. Based on this, the scattering matrix and the frequency responses were obtained.

Experimental

To fabricate the high frequency SAW devices, a layer of 60 nm thick PMMA was spin-coated onto an 128° Y-cut X-rotated $LiNbO_3$ substrate, which was heated and maintained at 180 ℃ for 5 minutes. Since the $LiNbO_3$ substrate is non-conductive, it would accumulate charges during the electron beam lithography process and thus the images would be distorted. To solve this problem, a thin

conductive layer of ESPACER was spin-coated at 4000 rpm in order to obtain a layer of ~40 nm on top of the PMMA. Then the electron beam exposure was conducted using an equipment of Raith 150 Two with an accelerating voltage of 30 kV. As the proximity effect of electron beams will cause a relatively large dose in the middle of UV exposure area and a smaller dose in the surrounding area, such a non-uniform dose distribution for the SAW IDTs would cause the failure of IDT fabrication. We used an improved electron-beam lithography lift-off process with a proximity effect correction (PEC) algorism. After the electron-beam exposure, the conductive polymer was removed by rinsing with deionized water for more than 30 seconds, and then the patterns were developed in a developer solution (MIBK: IPA=1:3) for 1 minute at -18 ℃. This was followed by immersing the sample inside isopropanol (IPA) for one minute at the same temperature, and finally quickly dried with N_2. After that, thermal evaporation was used for metallization, which was consisted of a Cr adhesion layer (1 nm) followed by an Au layer (~12 nm, 18 nm or 25 nm). Finally, the substrate was rinsed in acetone to form the SAW IDTs. The bus bar and wire pad (30 nm in total) of the SAW devices were fabricated using the conventional photolithography and lift-off processes. The number of IDT pairs (N) of all devices was 80 with the metallization ratio of 0.5 and the number of reflectors was kept as 50. The acoustic aperture of the IDT was 20λ and its direction is perpendicular to the cutting edge of $LiNbO_3$ wafer. The two-port IDTs have the ground-signal-ground (GSG) electrode configuration with the same ground (In supplementary materials), which is compatible for high frequency SAW measurement. The G pad and S pad have the same length of 100 μm and width of 100 μm, and the distance between these two pads is 150 μm. Different wavelengths λ of 400, 600, and 800 nm were designed and fabricated.

The fabricated SAW IDTs were characterized using a scanning electron microscope (SEM, model: Zeiss SIGMA HD). The frequency responses of the fabricated SAW devices were measured using an Agilent N5247A network analyzer equipped with a GSG probe station which can accurately record the frequency, amplitude, insertion loss and electromagnetic coupling coefficient (k_2^{eff}) of the SAW devices.

Figure 1(e) shows a schematic diagram of TNT sensing experiments. Firstly, we measured the resonant frequency of the SAW device with λ of 400 nm and remarked as S1 in Figure 1(e). Next, the molecules of p-aminobenzenethiol (PABT) were added on the surfaces of AuNPs (Au Nanoparticles: Au IDTs) through incubation of AuNP@LN (Au IDTs-lithium niobate structure) substrate within the PABT solutions for 2 hrs.[20] Here, the supramolecular host molecules functionalized with the self-assembled monolayer were bonded to the long chains of mercaptan or thioether, which were formed on the gold electrode through a strong interaction of Au-S bonds.[21, 22] The excess and free PABT molecules were then removed by spinning the SAW chip at 8000 r·min^{-1} for 5 min, and the chip was dried on a hot plate at 120 ℃ for 10 min. The resonant frequency of the device S2 was tested at this stage to verify the chemical linking of the PABT on the surface of AuNP@LN through Au-S bonds. Finally, 1.5 ml of 4.4×10^{-9} M TNT solutions diluted with methanol were dropped onto the surface of SAW detector and incubated for 2 hrs. The resonant frequency S3 was obtained after the free TNT solutions were removed.

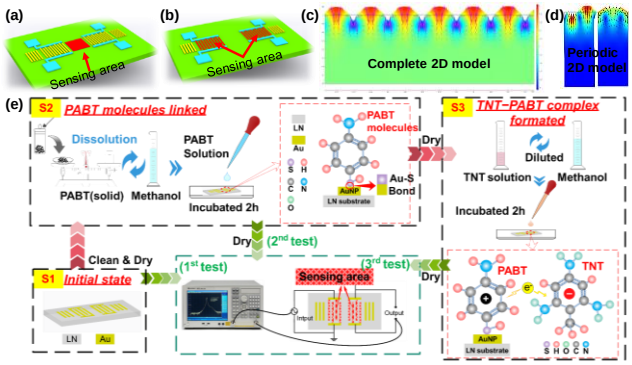

Figure 1. (a) Schematic illustration of sensing area of a conventional SAW sensor; (b) Schematic illustration of sensing area on the SAW IDT electrodes; (c) The simulated complete 2D model and the mode shapes of the SAW structure; (d) The simulated periodic 2D model and the mode shapes of the SAW structure; (e) A schematic diagram of the experiment process of TNT detection

Results and discussion

Mass loading effects at SAW propagation area and on SAW IDTs electrodes

Figure 2 shows the simulated results of resonant frequency differences between the mass loading effects on SAW propagation area and on SAW excited IDTs electrodes. It is clear that, for the case of SAW propagation area, with the mass loading increased from 0 μg mm^{-2} to 2.51 μg mm^{-2}, the frequency is only shifted from 8.72 to 8.68 GHz (corresponding to a shift of 0.04 GHz). Whereas the frequency is decreased from 8.72 GHz to 7.66 GHz (corresponding to a shift of 1.06 GHz) for the mass loading directly on the SAW IDTs electrodes. Results clearly show that for the same mass loading, the mass sensitivity obtained based on the SAW IDT electrodes is 26 times larger than that based on the SAW propagation area.

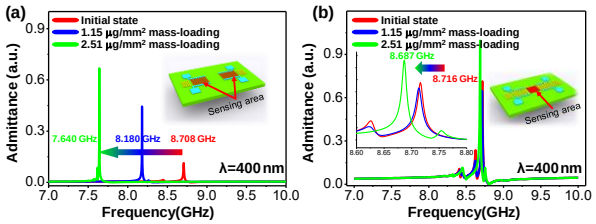

Figure 2. Simulated resonate frequency responses for mass loading effects of SAW device with a wavelength of 400 nm (a) mass loading effect on SAW IDTs, (b) mass loading effect at acoustic wave propagation area between two IDTs

Enhancing mechanism of electrode mass-loading effects on the SAW propagation properties

To investigate the enhancing mechanism of electrode mass-loading effect on the SAW propagation properties, different IDT thicknesses were made for the SAW devices with different wavelengths λ of 200 nm and 10 μm, on different substrates of $LiNbO_3$ and AlN/Diamond, respectively

(detailed information of the material properties used in simulation is provided in the supplementary materials).[23-25] Figure 3(a) shows the frequency responses of different Au electrode thicknesses for $LiNbO_3$ based SAW devices with the λ of 200 nm (nano-scale IDTs). Results show that for the IDTs' wavelength in nanoscale, the electrode mass loading has a significant effect on SAW frequency shift. With the Au electrode thickness increased from 10 nm to 200 nm, the resonant frequency is decreased by ~6.5 times, e.g., from 16.3 GHz to 2.5 GHz. However, when the λ value is in a micro-scale (eg. 10 μm, see Figure. 3(b)), the resonant frequency is only decreased by 6.7%, e.g., from 384 MHz to 358 MHz, at the same mass loading condition.

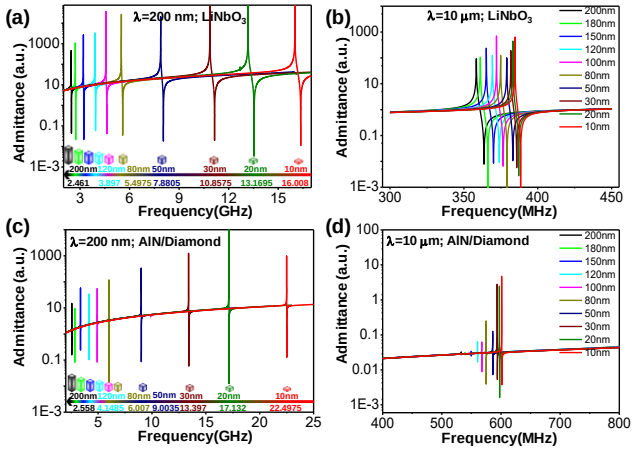

Figure 3. Effects of electrode thickness on SAW resonant frequency performance with different wavelengths and substrates. (a) wavelength of 200 nm and substrate of $LiNbO_3$; (b) wavelength of 10 μm and substrate of $LiNbO_3$; (c) wavelength of 200 nm and substrate of AlN/Diamond; (d) wavelength of 10 μm and substrate of AlN/Diamond

We have further simulated the SAW devices with the layered structure (AlN/Diamond) to verify this observation, and the results are shown in Figures. 3(c) and 3(d). With the Au electrode thickness increased from 10 nm to 200 nm, the resonant frequency is decreased by ~9 times and ~11.5%, for λ of 200 nm and 10 μm, respectively. These results clearly show that mass loading on the IDT electrodes has more significant effect on SAW frequency shifts when the wavelength is within nanoscale, and the higher resonant frequency will lead to enhanced electrode mass-loading effect on the SAW propagation properties.

To verify the correctness and accuracy of simulation results, we have also done the theoretical calculation of frequency responses using FEM/BEM for $LiNbO_3$ SAW device with the λ value of 200 nm, and the results are shown in Figure 4 (a). It is clear that, the frequency shifts have the same trend with those from the simulation and the frequency is decreased from ~16.3 GHz to ~2.5 GHz, by ~6.5 times, demonstrating the reliability of simulated results.

Frequency response characteristics of the SAW devices with different wavelengths of 200 nm, 400 nm, 600 nm, 800 nm,1000 nm and 10 μm for with different electrode thickness (10~200 nm) were further simulated using COMSOL Multiphysics 5.3a. Results shown in Figure 4(b) clearly indicate that with the same electrode thickness, the SAW device with a smaller wavelength will show a larger frequency shift. In addition, the smaller wavelength leads to a larger decrease of velocity for both the $LiNbO_3$ and AlN/Diamond SAW devices, as shown in Figures 4(c) and 4(d). These results demonstrate that the smaller period of IDTs has more pronounced mass-loading effect than the larger period of IDTs, which means electrode mass-loading effect on the IDTs in nanoscale is very suitable for ultrahigh frequency SAW sensing.

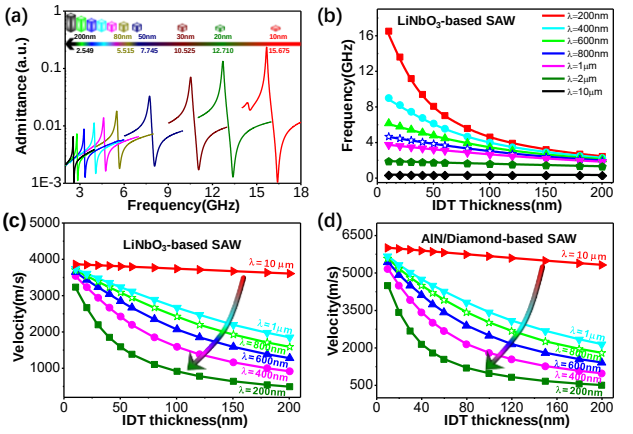

Figure 4. (a) FEM simulation results of frequency responses of a $LiNbO_3$-based SAW with λ of 200 nm; (b) Simulated characteristic of the frequency response of $LiNbO_3$-based SAW with different wavelengths and different electrode thicknesses; (c) Simulated acoustic velocity changes of $LiNbO_3$-based SAW with different wavelengths and different electrode thicknesses; (d) Simulated acoustic velocity changes of AlN/Diamond-based SAW with different wavelengths and different electrode thicknesses

To understand why the smaller wavelength leads to the larger mass loading effect, we have investigated the mechanism of electrode mass-loading effect on SAW IDTs by analyzing the periodic 2D piezo plane strain modes of SAW induced mass-loading. We simulated the particle vibration patterns of the SAW devices, and the results are illustrated in Figure 5. For the wavelength of 10 μm, when the electrode thickness is increased from 10 nm (1/1000 λ) to 200 nm (1/50 λ), the mode of particle vibration and geometrical variations of the electrode shape (acoustic wave field) do not show significant changes, because the electrode thickness is far less than the wavelength in micro-scale. However, when the wavelength is 200 nm (nanoscale), with the electrode thickness increased from 10 nm to 200 nm and the electrode thickness gradually increased up to 1λ, there is a relatively huge electrode mass loading for wavelength of 200 nm. Furthermore, with the electrode thickness increased from 10 nm to 200 nm, the particle vibration patterns of the SAW devices are dramatically changed. When the thickness is 10 nm, the particle vibration is mainly concentrated in the piezoelectric $LiNbO_3$ layer. However, when the electrode thickness is increased to 200 nm (e.g., 1λ), the particle vibration is more concentrated within the electrodes, which do not have the piezoelectric effect, thus leading to the sharp decrease of the velocity.

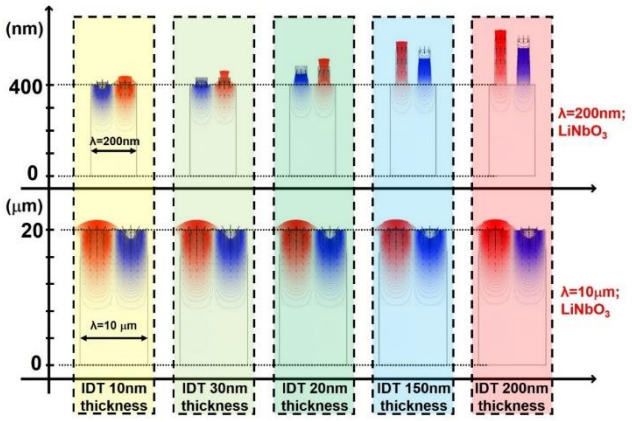

Figure 5. The simulated geometry and vibration modes of the $LiNbO_3$-basd SAW structure with a wavelength of 200 nm (the top row) and 10 μm (the bottom row)with different electrode thickness

Experimental demonstration of mass loading effects on SAW IDTs

To experimentally verify the giant mass-loading effect on IDT electrodes, we have fabricated high frequency SAW devices with the electrode thicknesses of 12, 18 and 25 nm. The first device with a thickness of 12 nm can be assumed to be the original SAW device without mass loading (e.g., assuming a mass loading effect of zero). The other two SAW devices can be assumed to have a mass loading of 1.16 μg·mm^{-2} and 2.51 μg·mm^{-2}, respectively. Fig. 6(a) demonstrates that we have optimized the EBL fabrication process and can fabricate the nanoscale IDTs with good repeatability (3 IDTs), uniformity and high quality. Figure 6(b) shows an optical image of complete two-port S AW devices in a GSG electrode configuration. The SAW IDTs with different wavelengths of 400, 600, and 800 nm were designed and fabricated as shown in Fig. 6(c) to 6(e).

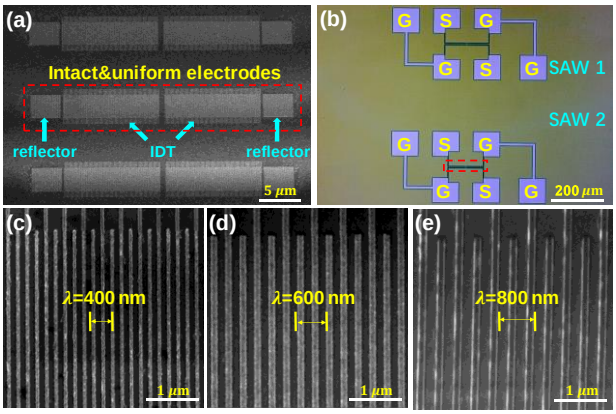

Figure 6. (a) The SEM image of high frequency IDTs with the number of IDT pairs (N) of 80 and reflectors of 50 by optimized EBL process (these three IDTs have the same wavelength of 400 nm, showing the good repeatability); (b) Optical image of high frequency SAW devices (SAW1 with a wavelength of 600 nm and SAW2 with a wavelength of 400 nm). (b). (c)~(e) SEM images of fabricated SAW IDTs with wavelengths of 400, 600, 800 nm.

Figures 7(a) to 7(c) show the reflectance spectra (S_{11}) of super high frequency SAW devices with different wavelengths and IDT thicknesses of 12 nm (0 mass loading), 18 nm (1.16 μg·mm^{-2} mass-loading) and 25 nm (2.51μg·mm^{-2} mass-loading), respectively. Results showed that all the SAW devices with different wavelengths present multiple wave modes. We used the COMSOL Multiphysics software to verify that these wave modes are Rayleigh modes and Longitudinal Leaky SAW (LLSAW) modes. With the wavelength decreased from 800 nm to 400 nm for the IDT thickness of 12 nm, the frequencies are gradually increased from the range of 4~8 GHz to the range of 7~13 GHz. Whereas the insertion loss and signal amplitude are decreased slightly, which is mainly due to the larger impedance of the IDTs with very narrow and slender IDT fingers. As we know that with such small features, it is difficult to achieve uniform widths of IDTs, thus the signals become worse. Nevertheless, the SAW device with the wavelength of 400 nm has obtained a good frequency signal at 12.8 GHz. As far as we have searched in the literature, this is the highest frequency for SAW device made on the lithium niobate substrate for sensing application.

As shown in Figure. 7(a), for the SAW devices with a wavelength λ of 400 nm, the Rayleigh frequencies with the IDT thicknesses of 12, 18 and 25 nm are 7.6 GHz, 7 GHz and 5.7 GHz, respectively, which means there is about 2 GHz frequency shift when the IDT thicknesses is increased from 12 to 25 nm. Whereas the frequency values of the corresponding LLSAW modes are decreased from 12.8 GHz, 11.5 GHz to 10.2 GHz, e.g., achieving a frequency shift of 2.6 GHz. Similarly, the frequencies of the SAW devices with the λ of 600 nm and 800 nm are also decreased sharply for both the Rayleigh modes and LLSAW modes (The detailed information of the tested device properties is provided in the supplementary materials).

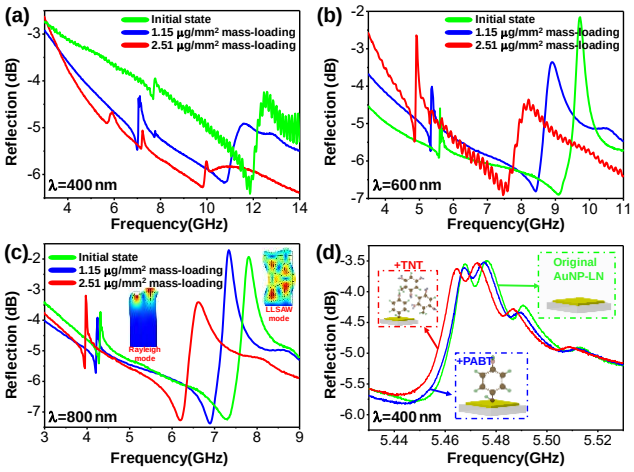

Figure 7. Frequency responses of the fabricated high frequency SAW device with the wavelength of (a) 400 nm, (b) 600 nm and (c) 800 nm (d) Frequency response of high frequency SAW device for TNT detection

We have further performed the simulations of frequency responses of super high frequency SAW devices with different wavelengths of 400, 600 and 800 nm and with the IDT thicknesses of 12, 18 and 25 nm. The simulation results showed that the frequency is decreased sharply when the IDT thickness is increased from 12 to 25 nm, which are compatible with the experimental results as

shown in the Supplementary materials. These results clearly demonstrate that the IDT electrode mass-loading has a significant effect on the SAW propagation properties of the nano-scale SAW devices.

It should also be noted that, when the IDT thickness is increased from 12 nm to 18 nm, the increased IDT mass values are: 14.84 pg for the λ of 400 nm, 33.39 pg for the λ of 600 nm, and 59.35 pg for the λ of 800 nm. Based on these results, we can conclude that the minimum detection mass in this work is 14.84 pg. As the corresponding frequency shift is about 0.6 GHz for this mass loading, the theoretical accuracy can be estimated as 2.47×10^{-11} ng for 1 Hz. This detection limit is quite small compared with those reported in literature,[26-28] which demonstrates the great potential for using this giant electrode mass loading effect in sensing applications.

The mass sensitivity of the SAW devices can be estimated as the frequency shift due to the mass change per area of A, (Δf/Δm/A).[29] where Δm is the change of mass loading, A is the area of the sensing region. The calculated sensitivity values for the Rayleigh and LLSAW mode are ~7309.1 MHz·mm^2·μg^{-1} and 8129.5 MHz·mm^2·μg^{-1}, respectively, for the SAW device with the wavelength λ of 400 nm. Furthermore, for the Rayleigh mode, the device with a smaller wavelength will have a larger mass sensitivity due to its higher resonant frequency. The higher-order harmonic mode has a larger sensitivity compared with that of the Rayleigh wave mode, also due to its higher frequency. The highest sensitivity of 8129.5 MHz·mm^2·μg^{-1} obtained in this study is $\sim8.9\times10^{11}$ times larger than that from a conventional QCM device (with a frequency of 5 MHz), and ~1000 times larger than a conventional $LiNbO_3$ SAW device with a frequency of 978 MHz, which have been listed in **Table 1.**

TABLE1. Characteristics of mass sensitivity SAW and QCM sensors

Reference	*Year*	*Type*	*Resonant frequency(GHz)*	*Sensitive of Mass sensing*
[26]	2010	SAW	0.121	0.1315MHz·mm^2·μg^{-1}
			0.978	8.23 MHz·mm^2·μg^{-1}
[27]	2017	SAW	0.144	32.42kHz/μg
[28]	2016	SAW	0.311	700kHz/μg
[30]	2007	QCM	0.006	6.1kHz·mm^2/μg
[31]	2013	QCM	0.005	7.11Hz/μg
[32]	2016	QCM	0.005	234.1 Hz/μg
This work	2019	SAW	11.867	6.351×10^6MHz/μg (8129.51903MHz·mm^2/μg)

TNT detection using SAW device

It is a great challenge but a crucial demand to develop SAW biochemical sensors to detect ultra-low concentrations of species in either gaseous or liquid environments (e.g., molecular biomarkers for diseases, toxic gases for environmental control and safety, and contaminants for water quality). In this section, we demonstrate the capability to use our newly developed $LiNbO_3$-based SAW devices for detection of TNT, which is one of the most commonly components of dangerous explosives. TNT has caused not only well-known security threat and cancer risk, but also an environmental concern due to contamination of soil and groundwater. It can be absorbed through skin, possibly resulting in anemia and abnormal liver functions.[33, 34]

The SAW device with the wavelength of 400 nm and Au electrode thickness of 12 nm was used for the TNT sensing, and the measurement results are shown in Figure 7(d). The original SAW resonator has a Rayleigh wave mode with a resonant frequency of 5.48 GHz. When the PABT was chemically bonded onto the surface of AuNP@LN through Au-S bonds, the resonant frequency was decreased to 5.4783 GHz. After the IDTs were treated with 1.5 ml 4.4×10^{-9} M TNT, the frequency was further decreased to 5.47143 GHz, e.g., with a shift of 6.87 MHz.

Results clearly indicate the great potential of the giant mass-loading effect for ultrasensitive sensing applications.

Conclusions

This paper investigates a new sensing mechanism based on the mass-loading effect directly on the IDT electrodes. Theoretical, simulation and experimental results show that the sensitivity of mass-loading effect on IDT electrodes is far greater than that on acoustic wave propagation area, due to the huge changes of acoustic field in the IDTs area. In addition, the nanoscale period (λ) of IDTs has more pronounced mass-loading effect than that of microscale λ, which means electrode mass-loading effect on IDTs in nanoscale is suitable to be applied to improve the sensitivity of the SAW sensors. Optimized nanofabrication processes were developed for the fabrication of extreme-high frequency SAW devices and 12 GHz Longitudinal Leaky SAWs was realized with an IDT finger width of 100 nm. With the Au electrode thickness increased from 12 nm to 25 nm (or with the corresponding mass-loading from initial state to 2.511 $\mu g \cdot mm^{-2}$), the Rayleigh mode resonant frequency was decreased from 7.77 GHz to 5.93 GHz, while the higher LLSAW mode was decreased from 11.87 GHz to 9.83 GHz. The estimated mass sensitivity for the two modes are 7309.1 $MHz \cdot mm^2 \cdot \mu g^{-1}$ and 8129.52 $MHz \cdot mm^2 \cdot \mu g^{-1}$. The obtained highest sensitivity value is 8.9×10^{11} times larger than that of a conventional quartz crystal balance (QCM with 5 MHz frequency) and ~1000 times higher than a conventional SAW device (with a frequency of 978 MHz), respectively. We also demonstrated that this giant mass-loading effect can be used as an excellent analytical platform for TNT detection with a low detection limit, indicating its great potential for ultrasensitive sensing applications.

AUTHOR INFORMATION

Corresponding Author

* Jian Zhou, Ph. D
Professor in College of Mechanical and Vehicle Engineering
State Key laboratory of Advanced Design and Manufacturing for Vehicle Body
Hunan University, Changsha 410082, P.R. China
Email: jianzhou@hnu.edu.cn.
* Huigao Duan, Ph. D
Professor in College of Mechanical and Vehicle Engineering
State Key laboratory of Advanced Design and Manufacturing for Vehicle Body
Hunan University, Changsha 410082, P.R. China
Email: duanhg@hnu.edu.cn.

Author Contributions

‡These authors contributed equally. / The manuscript was written through contributions of all authors. / All authors have given approval to the final version of the manuscript.

Acknowledgments

This work was supported by the Key Research Project of Hunan Province (2019GK2111, 2018GK2044), The UK Engineering and Physical Sciences Research Council (EPSRC) grants EP/P018998/1, Newton Mobility Grant (IE161019) through Royal Society and the National Natural Science Foundation of China. This work was also supported in part by Science and Technology Bureau Foundation of Changsha City (kh1904005).

REFERENCES

1. Ward, M. D.; Buttry, D. A., In Situ Interfacial Mass Detection with Piezoelectric Transducers. *Science* **1990,** *249* (4972), 1000-1007, doi:10.1126/science.249.4972.1000.
2. Boechler, N.; Eliason, J. K.; Kumar, A.; Maznev, A. A.; Nelson, K. A.; Fang, N., Interaction of a contact resonance of microspheres with surface acoustic waves. *Phys Rev Lett* **2013,** *111* (3), 036103, doi:10.1103/PhysRevLett.111.036103.
3. Vishinkin, R.; Haick, H., Nanoscale Sensor Technologies for Disease Detection via Volatolomics. *Small* **2015,** *11* (46), 6142-64, doi:10.1002/smll.201501904.
4. Ghosh, A.; Zhang, C.; Shi, S.; Zhang, H., High temperature CO2 sensing and its cross-sensitivity towards H2 and CO gas using calcium doped ZnO thin film coated langasite SAW sensor. *Sensor Actuat B-Chem* **2019,** *301*, doi:10.1016/j.snb.2019.126958.
5. Le, X.; Liu, Y.; Peng, L.; Pang, J.; Xu, Z.; Gao, C.; Xie, J., Surface acoustic wave humidity sensors based on uniform and thickness controllable graphene oxide thin films formed by surface tension. *Microsyst Nanoeng* **2019,** *5*, 36, doi:10.1038/s41378-019-0075-0.
6. Raj, V. B.; Nimal, A. T.; Parmar, Y.; Sharma, M. U.; Sreenivas, K.; Gupta, V., Cross-sensitivity and selectivity studies on ZnO surface acoustic wave ammonia sensor. *Sensor Actuat B-Chem* **2010,** *147* (2), 517-524, doi:10.1016/j.snb.2010.03.079.
7. Xuan, W.; He, M.; Meng, N.; He, X.; Wang, W.; Chen, J.; Shi, T.; Hasan, T.; Xu, Z.; Xu, Y.; Luo, J. K., Fast response and high sensitivity ZnO/glass surface acoustic wave humidity sensors using graphene oxide sensing layer. *Sci Rep* **2014,** *4*, 7206, doi:10.1038/srep07206.
8. Mazouz, Z.; Fourati, N.; Zerrouki, C.; Ommezine, A.; Rebhi, L.; Yaakoubi, N.; Kalfat, R.; Othmane, A., Discriminating DNA mismatches by electrochemical and gravimetric techniques. *Biosens Bioelectron* **2013,** *48*, 293-8, doi:10.1016/j.bios.2013.04.023.
9. Mujahid, A.; Afzal, A.; Dickert, F. L., An Overview of High Frequency Acoustic Sensors-QCMs, SAWs and FBARs-Chemical and Biochemical Applications. *Sensors (Basel)* **2019,** *19* (20), doi:10.3390/s19204395.
10. Ren, L.; Yang, S.; Zhang, P.; Qu, Z.; Mao, Z.; Huang, P. H.; Chen, Y.; Wu, M.; Wang, L.; Li, P.; Huang, T. J., Standing Surface Acoustic Wave (SSAW)-Based Fluorescence-Activated Cell Sorter. *Small* **2018,** *14* (40), e1801996, doi:10.1002/smll.201801996.
11. Glass, N. R.; Shilton, R. J.; Chan, P. P.; Friend, J. R.; Yeo, L. Y., Miniaturized Lab-on-a-Disc (miniLOAD). *Small* **2012,** *8* (12), 1881-8, doi:10.1002/smll.201102282.
12. Polla, D. L.; Francis, L. F., Processing and Characterization of Piezoelectric Materials and Integration into Microelectromechanical Systems. *Annu Rev Mater Res 28* (1), 563-597.
13. Luo, J.; Xie, M.; Luo, P.; Zhao, B.; Du, K.; Fan, P., A sensitive glucose biosensor without using glucose test strips based on ZnO/SiO2/Si surface acoustic wave device. *Mater Lett* **2014,** *130*, 14-16, doi:10.1016/j.matlet.2014.05.073.
14. Dickert, F. L.; Forth, P.; Bulst, W.-E.; Fischerauer, G.; Knauer, U., SAW devices-sensitivity enhancement in going from 80 MHz to 1 GHz. *Sensors & Actuators B Chemical* **1998,** *46* (2), 120-125, doi:10.1016/s0925-4005(98)00097-5.
15. He, X. L.; Li, D. J.; Zhou, J.; Wang, W. B.; Xuan, W. P.; Dong, S. R.; Jin, H.; Luo, J. K., High sensitivity humidity sensors using flexible surface acoustic wave devices made on nanocrystalline ZnO/polyimide substrates. *J Mater Chem C* **2013,** *1* (39), doi:10.1039/c3tc31126k.
16. Agostini, M.; Greco, G.; Cecchini, M., A Rayleigh surface acoustic wave (R-SAW) resonator biosensor based on positive and negative reflectors with sub-nanomolar limit of detection. *Sensor Actuat B-Chem* **2018,** *254*, 1-7, doi:10.1016/j.snb.2017.07.014.
17. Ventura, P.; Hode, J. M.; Lopes, B. In *Rigorous analysis of finite SAW devices with arbitrary electrode geometries*, 1995 IEEE Ultrasonics Symposium. Proceedings. An International Symposium, Seattle. WA. USA, Nov; IEEE: Seattle. WA. USA, 1995; pp 257-262.
18. Plessky, V. P.; Thorvaldsson, T., Periodic Green's function analysis of SAW and leaky SAW propagation in a periodic system

of electrodes on a piezoelectric crystal. *IEEE Transactions on Ultrasonics Ferroelectrics & Frequency Control* **1995,** *42* (2), 280-293.

19. Zhou, J.; Shi, X.; Xiao, D.; Wu, X.; Zheng, J.; Luo, J.; Zhuo, M.; Tao, X.; Jin, H.; Dong, S.; Tao, R.; Duan, H.; Fu, Y., Surface acoustic wave devices with graphene interdigitated transducers. *J Micromech Microeng* **2019,** *29* (1), doi:10.1088/1361-6439/aaee61.

20. Chen, N.; Ding, P.; Shi, Y.; Jin, T.; Su, Y.; Wang, H.; He, Y., Portable and Reliable Surface-Enhanced Raman Scattering Silicon Chip for Signal-On Detection of Trace Trinitrotoluene Explosive in Real Systems. *Anal Chem* **2017,** *89* (9), 5072-5078, doi:10.1021/acs.analchem.7b00521.

21. Diaz Aguilar, A.; Forzani, E. S.; Leright, M.; Tsow, F.; Cagan, A.; Iglesias, R. A.; Nagahara, L. A.; Amlani, I.; Tsui, R.; Tao, N. J., A hybrid nanosensor for TNT vapor detection. *Nano Lett* **2010,** *10* (2), 380-4, doi:10.1021/nl902382s.

22. Riskin, M.; Tel-Vered, R.; Lioubashevski, O.; Willner, I., Ultrasensitive Surface Plasmon Resonance Detection of Trinitrotoluene by a Bis-aniline-Cross-Linked Au Nanoparticles Composite. *J Am Chem Soc* **2009,** *131* (21), 7368-7378, doi:10.1021/ja9001212.

23. Caliendo; Cinzia, Theoretical investigation of high velocity, temperature compensated Rayleigh waves along AlN/SiC substrates for high sensitivity mass sensors. *Appl Phys Lett* **2012,** *100* (2), 021905.1-021905.3., doi:10.1063/1.3675619.

24. Fujii, S.; Odawara, T.; Yamada, H.; Omori, T.; Hashimoto, K. Y.; Torii, H.; Umezawa, H.; Shikata, S., Low propagation loss in a one-port SAW resonator fabricated on single-crystal diamond for super-high-frequency applications. *IEEE Trans Ultrason Ferroelectr Freq Control* **2013,** *60* (5), 986-92, doi:10.1109/TUFFC.2013.2656.

25. Tarumi, R.; Matsuhisa, T.; Shibutani, Y., Low temperature elastic constants and piezoelectric coefficients of LiNbO3 and LiTaO3: resonant ultrasound spectroscopy measurement and lattice dynamics analysis. *Japanese Journal of Applied Physics* **2012,** *51*, doi:10.1143/jjap.51.07ga02.

26. Hsu-Cheng, O.; Zaghloul, M., Synchronous One-Pole LiNbO3 Surface Acoustic Wave Mass Sensors. *IEEE Electron Device Lett* **2010,** *31* (5), 518-520, doi:10.1109/led.2010.2043636.

27. Ten, S. T.; Hashim, U.; Gopinath, S. C. B.; Liu, W. W.; Foo, K. L.; Sam, S. T.; Rahman, S. F. A.; Voon, C. H.; Nordin, A. N., Highly sensitive Escherichia coli shear horizontal surface acoustic wave biosensor with silicon dioxide nanostructures. *Biosens Bioelectron* **2017,** *93*, 146-154, doi:10.1016/j.bios.2016.09.035.

28. Hao, W.; Liu, J.; Liu, M.; Liang, Y.; He, S., Mass Sensitivity Optimization of a Surface Acoustic Wave Sensor Incorporating a Resonator Configuration. *Sensors (Basel)* **2016,** *16* (4), doi:10.3390/s16040562.

29. Thomas, S.; Cole, M.; Villa-López, F. H.; Gardner, J. W., High frequency surface acoustic wave resonator-based sensor for particulate matter detection. *Sensor Actuat A-Phys* **2016,** *244*, 138-145, doi:10.1016/j.sna.2016.04.003.

30. Rodriguez-Pardo, L.; Farina, J.; Gabrielli, C.; Perrot, H.; Brendel, R., Design considerations of Miller oscillators for high-sensitivity QCM sensors in damping media. *IEEE Trans Ultrason Ferroelectr Freq Control* **2007,** *54* (10), 1965-76, doi:10.1109/tuffc.2007.490.

31. Tan, F.; Huang, X.-H., Relations between Mass Change and Frequency Shift of a QCM Sensor in Contact with Viscoelastic Medium. *Chinese Phys Lett* **2013,** *30* (5), doi:10.1088/0256-307x/30/5/050701.

32. Kakenov, N.; Balci, O.; Salihoglu, O.; Hur, S. H.; Balci, S.; Kocabas, C., Weighing graphene with QCM to monitor interfacial mass changes. *Appl Phys Lett* **2016,** *109* (5), doi:10.1063/1.4960299.

33. Lichtenstein, A.; Havivi, E.; Shacham, R.; Hahamy, E.; Leibovich, R.; Pevzner, A.; Krivitsky, V.; Davivi, G.; Presman, I.; Elnathan, R.; Engel, Y.; Flaxer, E.; Patolsky, F., Supersensitive fingerprinting of explosives by chemically modified nanosensors arrays. *Nat Commun* **2014,** *5*, 4195, doi:10.1038/ncomms5195.

34. Qu, J.; Ge, Y.; Zu, B.; Li, Y.; Dou, X., Transition-Metal-Doped p-Type ZnO Nanoparticle-Based Sensory Array for Instant Discrimination of Explosive Vapors. *Small* **2016,** *12* (10), 1369-77, doi:10.1002/smll.201503131.

SYNOPSIS TOC